RESEARCH ACTIVITIES III
Department of Electronic Structure

III-A Synthesis and Characterization of Exotic Molecule Based Nano-Crystals of Metal Acetylides: Toward Carbon Encapsulated Metal Dot Array, Metal Nano-Networks and Metal-Carbon Hybrid Devices

Metal-carbon binary junctions are expected to exhibit interesting properties, such as Shottoky barrier rectification, optical and tunneling devices, and chemical protector against oxidation. Metal acetylides have the ionic bond between the metallic cation and the acetylide anion. In the simplest case, divalent metal cations (M^{2+}) form a fcc lattice structure with a C_2^{2-} anion between the two metal cations. The introduction of alkyl or aromatic group into the C_2 unit, producing R–C≡C$^-$, can generate organometallic cluster compounds $((R–C\equiv C^-)_aM^{a+})_n$, ($a$ = 1, 2), some of which can be isolated as a single crystal. These cluster compounds are soluble in organic solvent and provide solid films with nano-scale planarity by spin-coating method. Photoexcitation of metal-acetylides induces charge-neutralization reaction producing carbon-skinned metal particles, or metallic nanowires or nano-sheets covered with organic polymer matrices. This property leads us for application of photo-lithographical pattern generation of metallic circuits or magnetic arrays. On the other hand, the reaction mechanism of the photoreactions of the respective acetylide systems can be highly dependent on the electronic structure of metal atoms. We are also illuminating the mechanism of these reactions.

III-A-1 Electric Conductivity of Self-Assembled Copper Acetylide Nanowires and Nanocables

JUDAI, Ken; NISHIJO, Junichi; NISHI, Nobuyuki

[*Adv. Mater.* in press]

We have found that copper acetylide (C_2Cu_2) molecules self-assemble into ultra thin nanowires in an aqueous solution at room temperature, and annealing of the C_2Cu_2 nanowires converts to metallic copper nanowires encapsulated in carbon outer layers (nanocables). This copper nanocable core is extremely thin, in which only 8 Cu atoms can line up in the diameter. The electric conductivity of such thin wires becomes important for recent progress of electronic devices.

Actually, the current-voltage (*I-V*) measurement of the nanowires and nanocables was carried out by point-contact using an atomic force microscopy (AFM). Figure 1a illustrates a topological image of a C_2Cu_2 nanowire on Au substrate by AFM. The height observed by AFM was 5 ~ 6 nm, which corresponds to the diameter of a single C_2Cu_2 nanowire. By using a conductive cantilever, *I-V* properties could be observed with point-contacting through the nanowire. Figure 1b shows *I-V* characteristics of contacting onto the nanowire, and the nanocable after the annealing. Without nanowires and nanocables, the direct contact of the cantilever on the substrate showed a normal ohmic *I-V* property. As the cantilever was in contact with the nanowire, non-ohmic behavior was observed in *I-V* measurement. The band-gap of 0.5 ~ 1.5 eV was typically observed as the threshold voltages of the drastic increasing current.

When *I-V* characteristics of the converted nanocables was measured, much larger plateau of no current region was observed to be typically more than ~3 V. This indicates that the nanocable exhibits insulating character through the point-contact by AFM. Annealing of the semiconductive C_2Cu_2 nanowires produced Cu nanowires covered with carbon outer layers. The AFM cantilever was contacting to this carbon outer layers. The measurement by AFM proves that the nanocable is coated with microscopic insulator.

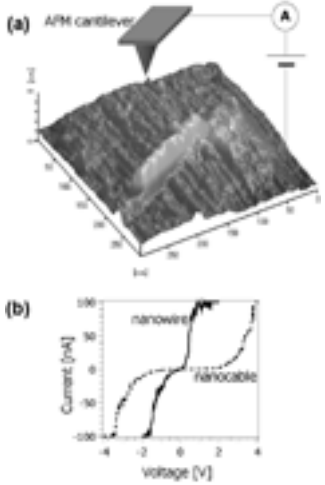

Figure 1. Electric conductive properties of C_2Cu_2 nanowires. (a) AFM image of a C_2Cu_2 nanowire on Au substrate. Schematic diagram is also supplemented for current-voltage (*I-V*) measurement. With using conductive cantilever (Au coated), current between the substrate and the cantilever through nanowires was measured. (b) *I-V* properties of nanowires and nanocables. Although the Au substrate showed ohmic *I-V* character, the C_2Cu_2 nanowire exhibited a non-ohmic property with a small band-gap (solid line). The converted Cu-nanocables covered with carbon provided insulating nature (dashed line).

III-A-2 Crystal Structure of C_2Cu_2 Nanowires by X-Ray Diffraction and DFT Calculation

JUDAI, Ken; NISHI, Nobuyuki

Copper acetylide (C_2Cu_2) molecules self-assembly into nanowires. The X-ray diffraction (XRD) measurement was performed to reveal stacking of C_2Cu_2 molecules in the nanowire. The sample of C_2Cu_2 nanowires exhibited several well-resolved peaks (Figure 1a). Peak widths of XRD measurement can be related to crystalline size by the Scherrer equation. Broader XRD peaks indicate smaller size. The coexistence of the sharp and broad signals for the crystals implies non-spherical crystalline structure of C_2Cu_2.

The density functional theory (DFT) calculation was carried out to assign the XRD spectrum. Various crystal structures have been reported for alkali metal acetylide compounds. We have optimized C_2Cu_2 crystal structure from these reported structures as initial geometries. The obtained structure with the lowest energy is illustrated in Figure 1c, which is essentially the same as the structure of C_2Li_2. The unit cell is orthorhombic (*Immm* No.71, Z = 2) with cell parameters of a = 3.39 Å, b = 4.58 Å, and c = 5.57 Å.

From the optimized crystal structure of C_2Cu_2, XRD spectrum can be simulated. Peak intensity can be calculated from the Lorenz-Polarization factors and the structure factors using DFT optimized unit cell. Peak width can be estimated by the Scherrer equation depending on the size of crystal. When a needle-like crystal (a = c = 5 nm, b = 40 nm) was assumed for their peak broadness, the dominant peaks of the observed XRD spectrum could be reproduced by the simulation (Figure 1b). This simulation suggests that the driving force of self-assembling nanowire production is originated in the highly anisotropic character of the C_2 unit. The b-axis of C_2Cu_2 crystal is the direction of the C_2 unit. The line width in the observed spectrum suggests that the crystal grows along b-axis more rapidly than the other axes.

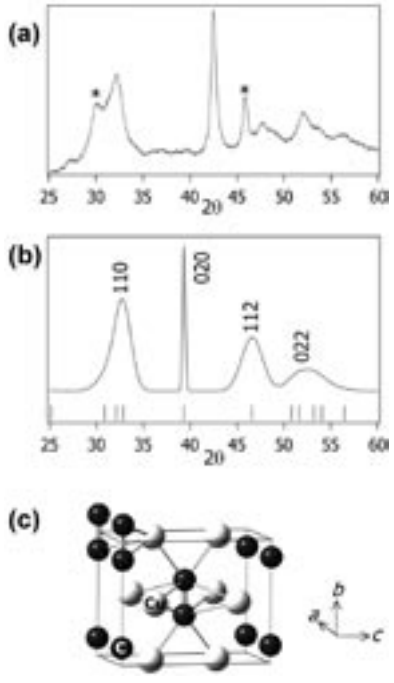

Figure 1. Crystal structure of C_2Cu_2 nanowires. (a) Powder XRD spectrum of C_2Cu_2 nanowires. The XRD results were acquired with X-ray of a Cu Kα line (0.154 nm). (b) Simulated XRD spectrum from the DFT calculated structure. The peak widths were estimated by the Scherrer equation with assumption of a needle shape (a = c = 5 nm, b = 40 nm). The dominant peaks of experimental XRD can be reproduced in the simulation, however, there are still unidentified peaks (labeled with *) of another crystal form. (c) DFT optimized structure of C_2Cu_2. The unit cell is orthorhombic and has body centered symmetry. C_2 units are coordinated with 4 Cu atoms in end-on sites and with 4 Cu atoms in side-on.

III-A-3 Photoconversion of Organometallic Cluster Thin Films to Metallic Copper-Sheets Sandwiched in Polymers

NISHI, Nobuyuki; NISHIJO, Junichi; JUDAI, Ken; OKABE, Chie; OISHI, Osamu

Generation of hot electrons in nanoparticles can be performed with efficient energy pumping from light harvesting π electron networks of organic matrices. Metallic copper is the best material for electronic conduction because of its low resistivity and enthalpy of fusion. $[Cu–C{\equiv}C–t\mathrm{Bu}]_{24}$ cluster molecules contain the light harvesting unit of ethynyl chromophore and the lowest excited π-d charge transfer triplet state. Photoexcitation of $[Cu–C{\equiv}C–t\mathrm{Bu}]_{24}$ films induces segregation of the crystals into metallic and organic phases and leads to evolve the metallic nanosheets sandwiched by organic polymers. High pressure mercury lamp irradiation for 2 hours produces copper nanoplates. KrF laser irradiation at a low power of 3 mJ/cm^2 also generates copper nanosheets, efficiently. Figure 1 displays the change of the TEM images of the film as functions of irradiated number of laser pulses, 120 shots (a), 1200 shots (b) and 9600 shots(c). In Figure 1-a, one can see the formation of nuclei of metallic particles. The wavy lattice patterns with 0.3 nm spacing are thought due to the alignment of the original cluster molecules and the disorder can be produced by the formation of metallic nuclei. Further irradiation causes planer crystals as seen in (b). The spacing of the lattice pattern is regular and the interval is 0.26 nm. At this stage, the crystals exhibit grain boundaries with several 10 nm scales. In the planes dominated with metallic plates, one can find whity matrix rooms composed of segregated ($t$butyl-ethynyl)$_n$ polymers. However, further photon impact fills these spaces with joining metallic particles or plates nearby located on the lower side and made them into larger crystalline sheets as seen in Figure 1-c, where not only the (111) plane but also the (110) plane of copper fcc crystals are seen with a lattice spacing of 0.26 and 0.36 nm, respectively.

In Figure1-d, we show schematic explanation of the evolution of small particles to a nanosheet in the photon field. The observed phenomenon can be explained by plasmon–plasmon interaction induced by the photon electromagnetic field and surface enhanced photochemical reactions of the residual ethynyl copper cluster molecules that may also supply heat for rearrangement of metal atoms in the joining particles or sheets. Energy supply to metallic particles from light harvesting organic matrices can be also important to increase the internal

temperature of the metals.

Figure 1-e displays a cross-sectional view of the film deposited on a polyimide film after the irradiation of KrF laser pulses (12000 shots). Photolithographic dot patterning observed by a SEM is shown in Figure 1-f that was made with a chromium photo-mask and washing the residual cluster molecules by hexane. Each dot is spaced at every 1 μm. The surface is covered with the polymer layer thinner than 50 nm that is easily removed by laser sputtering.

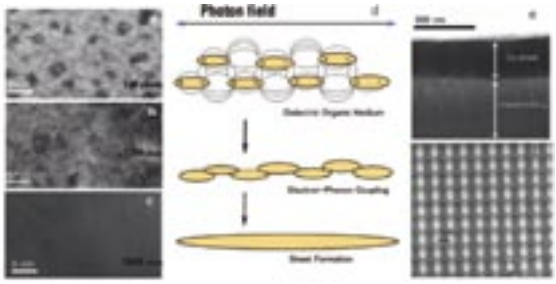

Figure 1. High resolution TEM images of the film as functions of irradiated number of laser pulses, 120 shots (a), 1200 shots (b) and 9600 shots(c). Laser energy density was 3 mJ/cm^2. (d) is schematic explanation of the evolution of small particles to a nanosheet in the photon field. (e) is a cross-sectional view of the film deposited on a polyimide film after the irradiation of KrF laser pulses (12000 shots). (f) is photolithographic copper-dot patterning obtained with a chromium photo-mask and washing the residual cluster molecules by hexane. Since, the copper surface is covered by thin polymer layer, copper parts look white.

III-A-4 Synthesis of Carbon-Encapsulated Nanoparticles *via* Thermal Decomposition of Metal Acetylide

NISHIJO, Junichi; OKABE, Chie; OISHI, Osamu; NISHI, Nobuyuki

[*Carbon* in press]

Carbon-encapsulated metal nanoparticles are promising materials for application in magnetic storage and battery due to their chemical stabilities. Though there are several methods of synthesizing the carbon-encapsulated nanoparticles such as arc discharge and thermal decomposition of hydrocarbons, the methods are not suitable for size-selective synthesis or mass production. Furthermore, the methods require a high temperature treatment which makes it difficult to synthesize carbon-encapsulated nanoparticles of metastable phases and low melting point metals. To solve these problems, we developed a new synthesis method for the carbon-encapsulated nanoparticles, where the carbon-encapsulated materials are formed by the low temperature thermal decomposition of the metal acetylide.

The acetonitrile suspension of metal chloride MCl_2 and calcium carbide CaC_2 sealed into the airtight vessel is heated to 240 °C for 12 h. In the solution, CaC_2 is gradually dissolved, and C_2^{2-} and M^{2+} form nanosized ionic cluster $(M^{2+}C_2^{2-})_n$ in the solution. Owing to the strong reducibility of C_2^{2-}, the cluster is converted into neutral metal-carbon cluster $(M^0C_2^0)_n$ by thermal energy. This neutral cluster is unstable because it can be regarded as metal-carbon supersatulated solid solution. As a result, metal atoms exclude the excess carbons and form carbon-encapsulated carbon-saturated metal nanoparticles. Figures 1 show the TEM images of carbon-encapsulated metal nanoparticles (M@C) of Sn, Pd, Ni and Co. As shown in the figures, each particle is covered with a carbon shell with the thickness of 2–6 nm which protects the metal or metal carbide core from the oxidation even in 1 M HClaq. The average core sizes depend on the metals; that is, 25, 8, 14 and 15 nm for M = Sn, Pd, Ni and Co, respectively.

The XRD patterns reveal the peculiar structures of the metallic cores. The core of Sn@C is pure metallic β-Sn, which reflects the instability of tin-carbide. On the other hand, other three metals prefer the carbide phases to metallic phases. The XRD pattern of Pd@C is explained as the sum of usual *fcc* and unusual *hcp* palladium carbide phases which has not been reported. In the case of M = Ni, Ni_3C phase is formed selectively. In contrast to the crystalline core structures mentioned above, the core of Co@C is almost all amorphous cobalt-carbon solid solution.

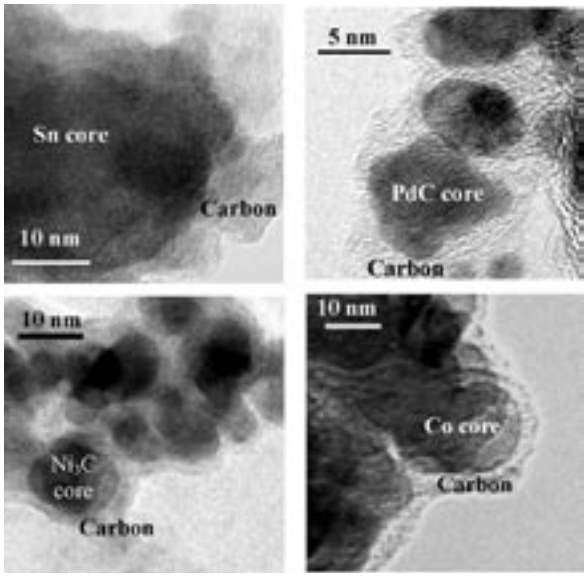

Figure 1. TEM images of carbon-encapsulated metal/metal carbide nanoparticles synthesized by thermal decomposition of metal-acetylide.

III-A-5 Synthesis, Structure and Magnetic Properties of a New Low-Spin Iron(III) Complex $[FeL_3]$ {L = $[HNC(CH_3)]_2C(CN)$}

NISHIJO, Junichi; NISHI, Nobuyuki

[*Eur. J. Inorg. Chem.* 3022–3027 (2006)]

High temperature treatment of acetonitrile with CaC_2 and $FeCl_2$ affords the new iron (III) S = 1/2 low-spin complex $[FeL_3]$ (L = $[HN{=}C(CH_3)]_2C(CN)$). The crystal structure and the inter-molecular overlap mode are largely affected by the crystal solvent ROH (R = Me, Et). In the $[FeL_3]$MeOH crystal, each MeOH molecule attracts $[FeL_3]$ complexes and disturb ligand–ligand interaction, resulting in the small overlap between adja-

cent complexes. On the contrary, [FeL_3] complexes form one-dimensional tunnel structure filled with EtOH molecules, where the inter-complex overlap is much larger as shown in Figure 1. The difference between the overlaps affects the inter-complex spin–spin interaction. The small overlap of [FeL_3]MeOH brings the negligibly small interaction, resulting in the Curie-like behavior of the spin. On the other hand, [FeL_3]EtOH behaves as singlet-triplet spin system with the interaction $2J/k_B$ = –7.5 K caused by stronger spin-spin interaction between adjacent complexes, which is originated from the large overlap between the π-electrons of the ligands. The EtOH crystal solvent can be easily removed only by evaporation owing to the tunnel structure of [FeL_3]EtOH, where the inter-complex interaction is reduced to negligibly small.

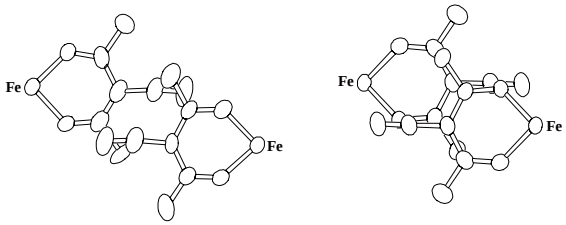

Figure 1. The inter-complex overlap mode of [FeL_3]MeOH (left) and [FeL_3]EtOH (right).

III-A-6 Preparation and Characterization of Gold Nanoparticles with Reactive Thiocarbonyls: A Proposal for Active Size Control of Nanoparticles

HINO, Kazuyuki[1]; NAKANO, Hirofumi[1],; ITO, Naomi[1]; MATSUSHITA, Machiko[1]; TAKAGI, Hideyuki[1]; NISHI, Nobuyuki
([1]Aichi Univ. Educ.)

[*Trans. Mater. Res. Soc. Jpn.* **31**, 525–528 (2006)]

Gold nanoparticles are prepared by using methyl-substitute 1,3-oxathiole-2-thione as a stabilizing reagent in the hydride reduction of tetrachloroaurate(III)ions. UV-vis absorption spectra and electron microscope observation show that the particle size can be controlled in a wide range from subnanometer to nanometer scale. Comparison of the results for these particles with those formed using methyl-substituted 1,2,4-trithiolane leads us to attribute the initial process of the formation of subnanometer-sized particles to the dimerization of 1,3-oxathiole-2-thione derivatives. In the reaction process, nascent particle surface is passivated with dimerization intermediates and the particle growth is terminated by sulfide formation.

III-B Ultrafast Dynamics and Scanning Tunneling Microscopy

Proton transfer and geometrical isomerization processes in electronic excited states are investigated with our pico-femto dual wavelength valuable systems. For the study of molecules on metallic or crystalline surface, very low temperature Scanning Tunneling Microscope (LT STM) system are now in use for collaboration with users in universities

III-B-1 Ultrafast Dynamics of Excited States of Chromium(III) Porphyrin Complexes in Solution

INAMO, Masahiko[1]; OKABE, Chie; NAKABAYASHI, Takakazu[2]; HOSHINO, Mikio[3]; NISHI, Nobuyuki
([1]Aichi Univ. Educ.; [2]Hokkaido Univ.; [3]RIKEN)

Cr(III) porphyrin complexes show variety of chemical reactivity and photophysical processes in their electronic excited states. In the present study, relaxation dynamics of the excited states following the Soret band excitation of the Cr(III) tetraphenylporphyrin complexes, [Cr(TPP)(Cl)(L)] (L = H_2O, Py, 1-MeIm), has been investigated using femtosecond time-resolved absorption spectroscopy in the toluene solution. The dynamics of the decay of the transient absorption spectra measured within a time domain of 400 ps is discussed with the various physical and chemical processes. In the case of [Cr(TPP)(Cl)(H_2O)], the biexponential decay of the initially populated excited state was observed with rate constants of $k_1 = 6.8 \times 10^{10}$ s^{-1} and $k_2 = 1.6 \times 10^9$ s^{-1}. These processes were assigned to the photodissociation of a H_2O ligand in the $^4S_1$ excited sate followed by the energy dissipation to electronically ground state [Cr(TPP)(Cl)]. On the contrary, the 1-MeIm complex [Cr(TPP)(Cl)(1-MeIm)], in which only the triplet excited state was observed using nanosecond transient spectra, shows a single exponential decay of the excited state. This was assigned to the decay of $^4S_1$ to T_1 with a rate constant of 3.8×10^9 s^{-1}. The excitation to S_2, the Soret band, occurs for 395 nm excitation followed by the intramolecular process of electronic, vibrational, and singlet-triplet relaxation with time scales of subfemtosecond, subpicosecond, and nanosecond, respectively, for a free base porphyrin. These findings indicate that the initially observed excited states in the present study may be $^4S_1$, and the S_2 to S_1 relaxation may be too fast to be observed in the present measurement. The lifetime of the $^4S_1$ excited states of [Cr(TPP)(Cl)(1-MeIm)] is much shorter than those of the porphyrin species that produce no paramagnetic ion due to the presence of the Cr(III) ion, but substantially longer than those of paramagnetic complexes such as [Cu(TPP)].

III-B-2 Scanning-Tunneling Microscopy, Near-Edge X-Ray-Absorption Fine Structure, and Density-Functional Theory Studies of N_2O Orientation on Pd(110)

WATANABE, Kazuo[1]; KOKALJ, Anton[2]; HORINO, Hideyuki[3]; RZEZNICKA, Izabela I.[2]; TAKAHASHI, Kazutoshi[3]; NISHI, Nobuyuki; MATSUSHIMA, Tatsuo[3]
([1]Fritz-Haber-Inst Max-Planck-Gesellschaft; [2]J. Stefan Inst.; [3]Hokkaido Univ.)

[*Jpn. J. Appl. Phys.* **45**, 2290–2294 (2006)]

The orientation of adsorbed N_2O on Pd(110) was studied by scanning tunneling microscopy, near-edge X-ray absorption fine structure (NEXAFS), and density functional theory. Below 14 K, N_2O(a) forms clusters extending along the $[1\bar{1}0]$ direction as well as monomers oriented along the [001] direction. In the clusters, N_2O is tilted with the terminal nitrogen bonding to the surface. The clusters are mobile at 14 K and stable at 8 K, whereas the monomers are stable at 14 K. In NEXAFS work at 60 K, remarkable anisotropy was found in the polarization dependence of π resonance, which was consistent with a mixture of the tilted and [001]-oriented forms.

III-C Spectroscopic and Dynamical Studies of Molecular Cluster Ions

Electron defficiency of molecular cluster cations can attract electron rich groups or atoms exhibiting charge transfer or charge resonance interaction in the clusters. This causes dynamical structural change such as proton transfer or ion-core switching in hot cluster ions or clusters in solution.

III-C-1 IR Photodissociation Spectroscopy of Hydrated Noble Metal Ions: Coordination and Solvation Structures

IINO, Takuro[1]; INOUE, Kazuya[1]; OHASHI, Kazuhiko[1]; MUNE, Yutaka[1]; INOKUCHI, Yoshiya[2]; JUDAI, Ken; NISHI, Nobuyuki; SEKIYA, Hiroshi[1]
([1]Kyushu Univ.; [2]Hiroshima Univ.)

Hydrated noble metal ions, $M^+(H_2O)_n$ (M = Cu, Ag), are studied by infrared photodissociation spectroscopy and density functional theory calculations. The third water in $Cu^+(H_2O)_3$ is hydrogen-bonded to one of the two waters coordinated to Cu^+, while all waters in $Ag^+(H_2O)_3$ are directly bonded to Ag^+. The difference in the coordination number is attributable to the different degree of *s-d* hybridization between Cu^+ and Ag^+.

III-D Development of High-Precision Coherent Control and Its Applications

Coherent control is based on manipulation of quantum phases of wave functions. It is a basic scheme of controlling a variety of quantum systems from simple atoms to nanostructures with possible applications to novel quantum technologies such as bond-selective chemistry and quantum computation. Coherent control is thus currently one of the principal subjects of various fields of science and technology such as atomic and molecular physics, solid-state physics, quantum electronics, and information science and technology. One promising strategy to carry out coherent control is to use coherent light to modulate a matter wave with its optical phase. We have so far developed a high-precision wave-packet interferometry by stabilizing the relative quantum phase of the two molecular wave packets generated by a pair of femtosecond laser pulses on the attosecond time scale. We will apply our high-precision quantum interferometry to gas, liquid, solid, and surface systems to explore and control various quantum phenomena.

III-D-1 Visualizing Picometric Quantum Ripples of Ultrafast Wave-Packet Interference

KATSUKI, Hiroyuki[1]; CHIBA, Hisashi[1]; GIRARD, Bertrand[2]; MEIER, Christophe[2]; OHMORI, Kenji[1]
([1]IMS and JST/CREST; [2]Univ. Paul Sabatier (Toulouse III))

[*Science* **311**, 1589–1592 (2006)]

Interference fringes in vibrating molecules are a signature of quantum mechanics, but are often so short-lived and closely spaced that they elude visualization. We have experimentally visualized dynamical quantum interferences, which appear and disappear in less than 100 femtoseconds in the iodine molecule synchronously with the periodic crossing of two counterpropagating nuclear wave packets. The obtained images have picometer and femtosecond spatiotemporal resolution, representing a detailed picture of the quantum interference.

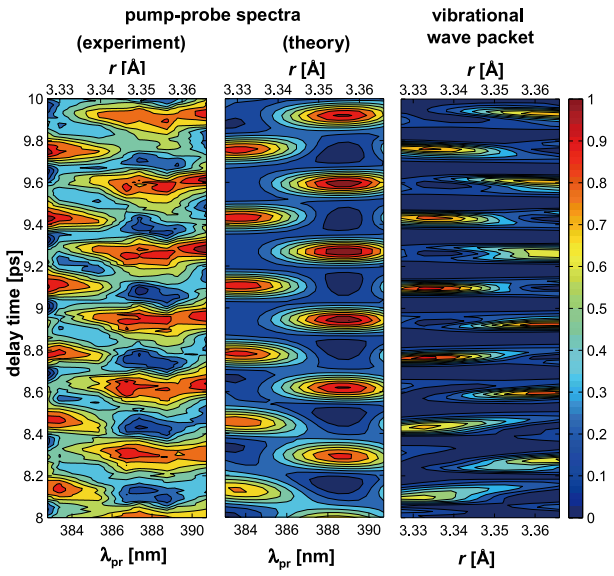

Figure 1. Contour plots of the experimental pump-probe signal (left), the simulated pump-probe signal (middle), and parts of the vibrational wave packet (right). The pump-probe spectra clearly reflect the spatiotemporal nodal structure of the wave-packet interferences.

[Reprinted with permission from *Science* **311**, 1589–1592 (2006). Copyright (2006) American Association for the Advancement of Science.]

III-D-2 Real-Time Observation of Phase-Controlled Molecular Wave-Packet Interference

OHMORI, Kenji[1]; KATSUKI, Hiroyuki[1]; CHIBA, Hisashi[1]; HONDA, Masahiro[2,3]; HAGIHARA, Yusuke[2,3]; FUJIWARA, Katsutoshi[3]; SATO, Yukinori[2,3]; UEDA, Kiyoshi[2,3]
([1]IMS and JST/CREST; [2]JST/CREST; [3]Tohoku Univ.)

[*Phys. Rev. Lett*. **96**, 093002 (4 pages) (2006)]

The quantum interference of two molecular wave packets has been precisely controlled in the *B* electronic state of the I_2 molecule by using a pair of fs laser pulses whose relative phase is locked within the attosecond time scale and its real time evolution has been observed by another fs laser pulse. It is clearly observed that the temporal evolution changes drastically as a function of the relative phase between the locked pulses, allowing us to read both amplitude and phase information stored in the wave functions of the molecular ensemble.

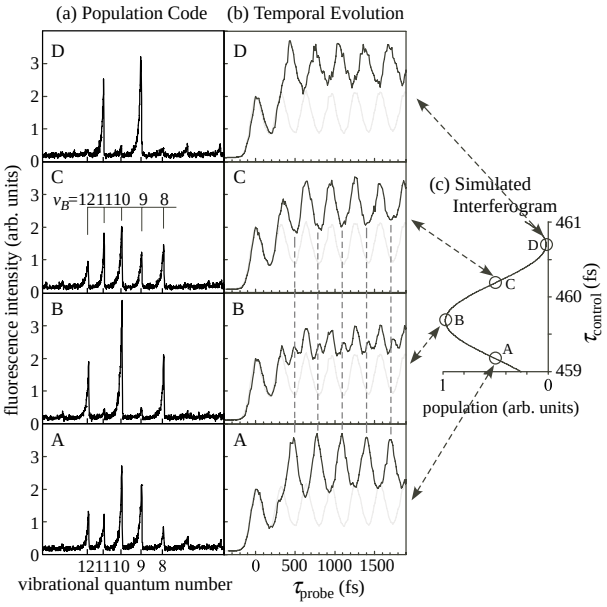

Figure 1. Wave packet interference measured and simulated with the pump and control delay $\tau_{control}$ tuned to ~1.5 T_{vib} (~460 fs), where T_{vib} is a classical vibrational period of I_2. (a) *E–B* excitation spectrum, which we call the "POPULATION CODE," measured by scanning the wavelength of the ns probe pulse delayed by ~35 ns from the pump and control pulses. The relative phase θ_{p-c} of the pump and control pulses is increased in steps of ~π/2 in going from code A to code D. (b) Real time evolutions of the wave-packet interference measured with the same θ_{p-c}'s as for codes A-D. The shaded trace is the evolution measured without the control pulse and is displayed for reference. Each trace is a summation of four repeated scans. The origin of the probe delay (τ_{probe} = 0) denotes a position of the top of the first undulation in each measured trace. The vertical scaling of each trace is arbitrary and is normalized by the height of its first undulation. (c) Simulation of $\tau_{control}$-dependence of the population of v_B = 10. The arrows stand for approximate correspondences in θ_{p-c}, and not in the absolute values of $\tau_{control}$.
[Reprinted with permission from *Phys. Rev. Lett*. **96**, 093002 (4 pages) (2006). Copyright (2006) American Physical Society.]

III-D-3 Implementation of Quantum Gate Operations in Molecules with Weak Laser Fields

TERANISHI, Yoshiaki[1]; OHTSUKI, Yukiyoshi[1]; HOSAKA, Kouichi[2]; CHIBA, Hisashi[2]; KATSUKI, Hiroyuki[2]; OHMORI, Kenji[2]
([1]Tohoku Univ. and JST/CREST; [2]IMS and JST/CREST)

[*J. Chem. Phys.* **124**, 114110 (9 pages) (2006)]

We numerically propose a way to perform quantum computations by combining an ensemble of molecular states and weak laser pulses. A logical input state is expressed as a superposition state (a wave packet) of molecular states, which is initially prepared by a designed femtosecond laser pulse. The free propagation of the wave packet for a specified time interval leads to the specified change in the relative phases among the molecular basis states, which corresponds to a computational result. The computational results are retrieved by means of quantum interferometry. Numerical tests are implemented in the vibrational states of the B state of I_2 employing controlled-NOT gate, and 2 and 3 qubits Fourier transforms. All the steps involved in the computational scheme, *i.e*., the initial preparation, gate operation, and detection steps, are achieved with extremely high precision.

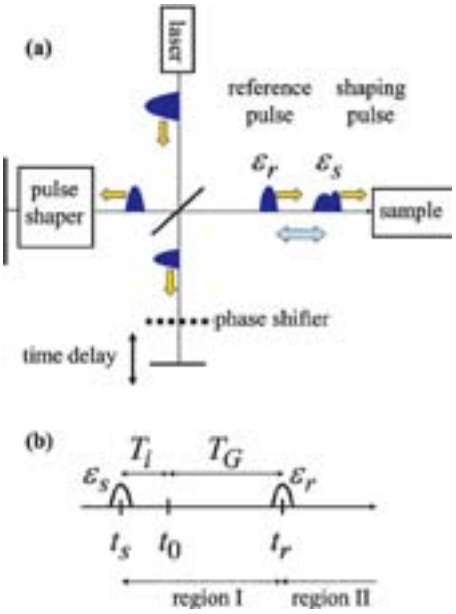

Figure 1. (a) Schematic of the experimental setup. (b) Pulse sequence for quantum computation. The times, t_s, t_0, and t_r, specify the temporal peak of the shaping pulse, the initial separation time, and the temporal peak of the reference pulse, respectively. The time intervals are referred to as the input preparation time $T_i = t_0 - t_s$ and the gate operation time $T_G = t_r - t_0$.
[Reprinted with permission from *J. Chem. Phys.* **124**, 114110 (9 pages) (2006). Copyright (2006) American Institute of Physics.]

III-E Quantum-State Manipulation of Molecular Motions

Molecules in gas phase undergo translational, rotational and vibrational motions in a random manner, and the total molecular system is a statistical ensemble that contains a number of molecules in many different states of motions. This research group aims to establish methods to manipulate the quantum-state distribution pertinent to molecular motions, by utilizing the coherent interaction with laser lights. Three complement methods are now being explored for manipulation of molecular motions. The first method exploits an impulsive interaction with ultrafast intense laser light to transform the initial distribution into an arbitral non-equilibrium one. We have succeeded in applying the method to nonadiabatic rotational population transfer in various molecular systems. The second one employs creation and detection of molecular wavepackets by fs pump–probe experiments. Experimental methods newly developed in this laboratory have been applied to probing vibrational wavepackets associated with internal rotation of jet-cooled polyatomic systems. The third one utilizes an adiabatic interaction to achieve the complete population transfer, by which all the molecules are launched into states with high excitation of vibrations or rotation. We have constructed ns laser systems with sufficiently high frequency resolution to drive the adiabatic coherent interaction. Along the development of the instruments, appropriate candidates for the quantum-state adiabatic manipulation are searched. Laser spectroscopic studies are carried out to explore energy-level structure of the intermolecular vibrations in molecular clusters containing benzene.

III-E-1 Nonadiabatic Population Transfer by Intense Femtosecond Laser Light

HASEGAWA, Hirokazu; OHSHIMA, Yasuhiro

A new vacuum chamber was constructed for the study of nonadiabatic population transfer processes induced by intense fs laser light, and has been utilized to explore the rotational excitation of NO. A fundamental output (~800 nm, ~120 fs duration, and < 1 mJ/pulse) of a titanium-sapphire laser was introduced to transiently align NO molecules, which were initially jet-cooled to < 2 K where states with J = 0.5 were only populated. Rotational distribution after the impulsive excitation was monitored by two-photon resonance enhanced ionization by ns laser pulses through the A–X(0,0) transition. States with up to J = 8.5 were populated through the nonadiabatic transfer process, and characteristic population alternation in J was identified. A model calculation has been performed to quantitatively explain the observations. The excitation is achieved through a ladder climbing mechanism by Raman process with $\Delta J = \pm 1$ and ±2. Because the transition probabilities with $\Delta J = \pm 2$ are much larger than those with $\Delta J = \pm 1$ and the initial distribution is restricted only to J = 0.5, populations in J = 2.5, 4.5, 6.5, … become superior.

For further detailed insight into the nonadiabatic rotational excitation, experiments utilizing double excitation pulses with an appropriate delay in time have been performed. Population of each rotational state changes oscillatory against the delay, with frequency components matching with rotational-energy differences. It has been shown the rotational states are grouped into two, in which states strongly couples *via* $\Delta J = \pm 2$ matrix elements to form the coherent superposition. The two groups are weakly coupled to each other *via* $\Delta J = \pm 1$ matrix elements. Such an excitation process is typical to molecules in degenerate states.

In addition to the simple diatomic molecule NO, much larger molecular systems, *i.e.*, benzene and styrene, have been examined for the nonadiabatic rotational excitation by intense short laser pulses. These successful applications demonstrate the potential of the present method in manipulation of quantum-state distribution of various types of molecules.

III-E-2 Wavepacket Observation of Methyl Internal Rotation in Substituted Toluenes

KITANO, Kenta[1]; MIYAZAKI, Mitsuhiko[2]; HASEGAWA, Hirokazu; OHSHIMA, Yasuhiro
([1]Kyoto Univ.; [2]IMS and Tokyo Tech)

Femtosecond (fs) time-domain experiments have been performed in the S_1–S_0 origin regions of jet-cooled *o*-fluorotoluene and *m*-cresol to explore the wavepacket dynamics associated with internal rotation of the methyl group. The COIN (Coherence Observation by Interference Noise) method, a variant of fs interferometry,[1)] has been applied to observe quantum beats, of which frequencies correspond to differences between vibronic transitions. Time-resolved fluorescence depletion (TRFD)[2)] has been implemented in fs domain for the first time, where change in excited-state population induced by the pump–dump process was monitored as fluorescence depletion. In *o*-fluorotoluene, quantum interferences in S_1 were exclusively observed in the TRFD spectrum. Comparison with the COIN and TRFD data allows us to reconstruct the vibronic band structure without ambiguity. On the other hand, TRFD spectrum of *m*-cresol was dominated by quantum beats in S_0, because the separations between internal-rotation levels are smaller in S_0 than in S_1. The modulation amplitude of the beats reached to 5% of the total fluorescence, indicating substantial coherent population transfer to excited internal-rotation states in S_0 *via* Rabi oscillation induced by the pump pulse.

References

1) O. Kinrot, I. Sh. Averbukh and Y. Prior, *Phys. Rev. Lett.* **75**, 3822 (1995).
2) M. J. Côté *et al.*, *J. Chem. Phys.* **90**, 2865 (1989); G. V. Hartland, L. L. Connell and P. M. Felker, *J. Chem. Phys.* **94**, 7649 (1991).

III-E-3 Development of High-Resolution Coherent Pulsed Lasers

OHSHIMA, Yasuhiro; SUMA, Kosuke

We are constructing a pulsed laser system with Fourier-transform (FT) limited resolution for quantum-state manipulation by coherent light–matter interaction, such as stimulated Raman adiabatic passage. In the system, the output from a cw ring titanium-sapphire laser seeds a pulsed dye amplifier pumped by a single-mode Nd:YAG laser. The laser system delivers the output power of 30 mJ/pulse at around 780 nm, with spectral bandwidth of 200 MHz (< 0.007 cm^{-1}). This fundamental output is tripled by nonlinear crystals to have UV radiation at 260 nm, which is suitable to excite S_1–S_0 transitions of the benzene molecule and its van der Waals clusters.

In addition to the pulsed amplifier system, an all solid-state pulsed laser system based on the optical parametric oscillation (OPO) pumped by the Nd:YAG laser is now in under construction. The OPO system is injection-seeded by an extra-cavity cw diode laser. For stable external seeding operation, the ring-type cavity is adopted for the OPO. The frequency locking mechanism for the cavity is now designed and constructed. This OPO system will deliver the almost FT-limited ns pulse with > 10 mJ/pulse at 520 nm.

III-E-4 Laser Spectroscopy of the van der Waals Vibrations of Benzene–Water

MIYAKE, Shin-ichiro[1]; MIYAZAKI, Mitsuhiko[2]; OHSHIMA, Yasuhiro
([1]Kyoto Univ.; [2]IMS and Tokyo Tech)

Benzene-water is a prototypical system containing the π hydrogen bond. We have recently examined in detail the vibronic spectra of various isotopomers of the benzene–water 1:1 cluster pertaining to the S_1–S_0 6_0^1 transition of the benzene moiety, recorded by utilizing resonance two-photon ionization (R2PI) time-of-flight mass spectrometry. UV-UV hole-burning measurement has been performed to observe weak vibronic bands, which are buried in the R2PI excitation spectrum by background signals due to fragmentation of higher clusters. For the H_2O isotopomer, bands from the $m = 0$ and ± 1 internal-rotation states were separately observed by probing split components in the 6_0^1 origin. A dozen of bands with intermolecular mode excitation clearly appeared in the region up to 160 cm^{-1}. Observed level structure was compared with the 6D dynamical calculation by Felker and co-workers[1)] based on the model potential by Karlström *et al.*[2)] Levels pertaining to the vdW stretching and bending modes show reasonable agreements between observation and calculation, while states probably associated to the 3D internal rotation of water unit exhibit extremely large discrepancies. This result indicates the necessity for the substantial refinement in the model potential, especially for its anisotropic part (*i.e.*, angular dependence on the 3D internal-rotation coordinates).

References

1) W. Kim *et al.*, *J. Chem. Phys.* **110**, 8461 (1999).
2) G. Karlström *et al.*, *J. Am. Chem. Soc.* **105**, 3777 (1983).

III-F Spectroscopy of Jet-Cooled Aromatic Molecules and Photochemical Reaction of Aza- and Thio-Substituted Nucleobases

The phenomena of energy relaxation in isolated molecules have been essential issue in chemical dynamics over many decades. The laser spectroscopy coupled with the jet expansion gives us much information on molecular structure and relaxation processes. The substituent of the $-NH_2$ or $-SCH_3$ group should play an important role for the structure and the relaxation processes in their excited states.

Transient molecules such as excited states and chemical intermediates, which can be generated with laser irradiation, have been detected by laser flash photolysis. Time-resolved photothermal techniques are powerful to study nonradiative processes because they can detect the released heat from excited molecules directly with high sensitivity. Combination of photoexcited and photothermal methods will give us detailed information on photophysical and photochemical dynamics of intermediates, as well as excited states.

III-F-1 Conformation of 2-Aminoindan in a Supersonic Jet: The Role of N–H···π Hydrogen Bonding

IGA, Hiroshi[1]; ISOZAKI, Tasuku[1]; SUZUKI, Tadashi[1]; ICHIMURA, Teijiro[2]
([1]Tokyo Tech; [2]IMS and Tokyo Tech)

Weak intramolecular hydrogen bonding has attracted considerable attention of many researchers because it would govern chemical and physical properties of flexible molecules. Previously, we studied 1-aminoindan in a supersonic jet expansion, and two rotational isomers stabilized by an intramolecular N–H···π hydrogen bonding were observed. To further understand the interaction we investigate the effect of the position of the substitution. We measured laser-induced fluorescence (LIF) and dispersed fluorescence spectra of 2-aminoindan (2-AI). Three series of bands in the LIF spectrum were observed, and were assigned to the corresponding conformational isomers with the aid of *ab initio* calculation at the MP2/6-311+G(d,p). A hydrogen atom of the amino group in the most stable conformer points toward the benzene ring, suggesting the contribution of an intramolecular hydrogen bonding between the hydrogen atom and the π-electron of the benzene ring. The contribution of the extremely weak intramolecular hydrogen bonding to the molecular structure of 2-AI was elucidated. The strength of the hydrogen bonding of 2-AI was discussed in detail.

III-F-2 Conformation of Thioanisole in a Supersonic Jet

NAGASAKA, Mariko[1]; ISOZAKI, Tasuku[1]; SUZUKI, Tadashi[1]; ICHIMURA, Teijiro[2]
([1]Tokyo Tech; [2]IMS and Tokyo Tech)

It is suggested that thioanisole has a planar and perpendicular conformers with respect to the rotation of methylthio group around the $C(sp^2)$–S bond. Despite of many experimental and theoretical attempts, the most stable conformer and potential energy curves are still of subject because the experimental and theoretical results are not consistent each other. In this study, to elucidate the molecular structure of thioanisole in S_0 and S_1 states we measured the laser-induced fluorescence (LIF) and dispersed fluorescence (DF) spectra of thioanisole in a supersonic jet. We can firmly conclude that the most stable conformer in the S_0 and S_1 states is the planer conformer. In the LIF spectrum, low-frequency out-of-plane torsional mode, which is only allowed if their quantum numbers change by an even number, was observed relatively intensive. It is suggested that in the S_1 state structure of thioanisole is slightly twisted outside the benzene ring.

III-F-3 Excited-State Dynamics of 6-Azauracil with UVA Light Irradiation

KOBAYASHI, Takashi[1]; HARADA, Yosuke[1]; SUZUKI, Tadashi[1]; ICHIMURA, Teijiro[2]
([1]Tokyo Tech; [2]IMS and Tokyo Tech)

Analogues of nucleobases have been paid much attention because of distinct properties to originals. Aza-nucleobase, incuding a N atom into the skeleton of the nucleobase molecule, is one of the well-known analogues for anti-neoplastic and fungistatic properties. For the wide application, it is important to obtain information on relaxation and reaction mechanism of photo-excited nucleobase analogues.

We have measured transient absorption spectrum of 6-Azauracil (6-AU) in deaerated acetonitrile with the nanosecond 248 nm laser. Immediately after the laser shot, an absorption band peak at 320 nm and a broad absorption band at 500–700 nm were observed. The absorption bands are assigned to the lowest excited triplet (T_1) state of 6-AU (T–T absorption). The T–T absorption decayed with the rate constant of 5.0×10^6 s^{-1}. With the time-resolved thermal lensing experimant, it was found that the triplet 6-AU produces singlet oxygen ($^1\Delta_g$) efficiently.

III-F-4 Ultrafast Excited-State Dynamics of 4-Thiothymidine in Aqueous Solution

HARADA, Yosuke[1]; SUZUKI, Tadashi[1]; ICHIMURA, Teijiro[2]; OKABE, Chie; NISHI, Nobuyuki
([1]Tokyo Tech; [2]IMS and Tokyo Tech)

Thionucleobases and thionucleosides have received renewed attention because of high sensitivity to UVA light (320–400 nm) in which region normal DNA constituents are transparent. 4-Thiothymidine (s^4-TdR), an analogue of the naturally occurring nucleoside thymidine, has strong absorption in the UVA region. Recently it was reported that s^4-TdR can be readily incorporated into cellular DNA and that low doses of UVA light can easily inflict lethal damage on the DNA containing s^4-TdR, causing cell death. The synergistic use of s^4-TdR and UVA light offers a novel approach to cancer treatment. Apparently, electronically excited state of s^4-TdR is at the initial and crucial stage of the UVA-induced cell killing, and thus photophysical and photochemical studies of s^4-TdR would be of great significance. Recently, we elucidated that the major process of deactivation of photoexcited s^4-TdR is intersystem crossing (ISC) to triplet manifolds, and the quantum yield for ISC of s^4-TdR to be unity. In this study, ultrafast transient absorption measurement was performed with the pump-probe technique in order to obtain more detailed information on the S → T ISC process.

We have measured a time profile of the transient absorption of s^4-TdR in aqueous solution (pH 7.4) monitored at 570 nm obtained by 263 nm femtosecond laser excitation. The transient absorption emerged within the instrumental response time (< 0.50 ps) and decayed with the decay time of 10 ps. We have also measured a time profile of the transient absorption of thymidine (TdR) under the same experimental condition for s^4-TdR. The transient absorption emerged by the excitation decayed immediately to the initiate level, and it was found the transient should decay with time constant of equal or faster than 0.50 ps. For both cases of s^4-TdR and TdR, the observed transients should be assigned to be their excited singlet states, and the decay rate constants of the transient absorption should be regarded as the lifetime of the excited singlet states. It was clarified that s^4-TdR decays much slowly (10 ps) compared with TdR (0.5 ps), and the S → T ISC process of s^4-TdR should take place with time of approximately 10 ps.

III-G Photochemical Reactions in Microreactors

In the last decade, microreaction system has developed using the features unique to microspace such as short molecular diffusion distance, excellent heat transfer characteristics, laminar flow, and large surface-to-volume ratio. Although microreaction systems are successfully examined in a wide range of applications of analytical and organic chemistry, there are only several reports on photoreactions in microreactors as described in the following section. We can expect microreactors to exhibit higher spatial illumination homogeneity and better light penetration through the entire reactor depth in comparison to large-scale reactors. Thus, we are investigating applications of microreactors on organic photoreactions.

III-G-1 Application of Microreactors for Photoreactions

ICHIMURA, Teijiro[1]; MATSUSHITA, Yoshihisa[2]; SAKEDA, Kosaku[2]; SUZUKI, Tadashi[2]
([1]IMS and Tokyo Tech; [2]Tokyo Tech)

[*Photoreactions*, in *Microchemical Engineering in Practice*, T. R. Dietrich, Ed., Blackwell Publishing (2006)]

We investigated effects of residence time, reaction temperature, laser power, and excitation wavelength on photosensitized enantio- and diastereo-differentiating reactions in microreactors. Photonic efficiencies of model reactions were considerably larger than those in conventional batch reactors. Further, the yield of photosensitized diastereodifferentiating addition of methanol to terpenes was greatly improved in the microreactor.

Photocatalytic oxidation of endocrine disruptors, reduction of organic compounds, and amine alkylation processes were investigated in a microreactor with immobilized photocatalytic TiO_2 layer. Apparent reaction rates in microreactors were much larger than those in conventional batch reactors. A photocatalytic process of N-alkylation of benzylamine in alcohol media was successfully observed by using microreactors with immobilized Pt-free TiO_2 as well as Pt-loaded TiO_2, while it has been reported that the N-alkylation didn't occur by the irradiation of Pt-free TiO_2 in conventional batch reactors. The study on the oxidation process of olefins by using a multiphase-photocatalytic microreactor was also reported.

III-G-2 Photocatalytic Reduction in Microreactors

MATSUSHITA, Yoshihisa[1]; KUMADA, Shinji[1]; WAKABAYASHI, Kazuhito[1]; SAKEDA, Kosaku[1]; ICHIMURA, Teijiro[2]
([1]Tokyo Tech; [2]IMS and Tokyo Tech)

[*Chem. Lett.* **35**, 410–411 (2006)]

Photocatalytic reduction of benzaldehyde and nitrotoluene in microspace was investigated by using a microreactor with immobilized titanium dioxide. Since a photocatalytic reaction takes place on an irradiated titanium dioxide surface, a microfabricated reactor which has a large surface-to-volume ratio must prove its advantages on the reaction.

Photoreduction was carried out with a microreactor made of quartz which has a microchannel of 500 μm width, 100 μm depth, and 40 mm length. The bottom

and side walls of the microchannel were coated with a photocatalytic TiO_2 layer. To appear the advantages of the miniaturized reaction vessel, a light source of minimal space and lower photon cost is suitable for the microreaction system. We employed UV light emitting diodes (UV-LEDs) for the excitation light source of photocatalyst. Alcohol solutions of benzaldehyde or nitrotoluene saturated with nitrogen were introduced to the microreactor with a syringe pump and irradiated with UV-LEDs. The reactions proceeded within 60 s to yield 10.7% of benzylalcohol from benzaldehyde and 45.7% of *p*-toluidine from *p*-nitrotoluene by the excitation of 365 nm UV-LED. The results suggest the possibilities of a catalytic microreaction system on organic photoreactions.

III-H Coherent Phonon Dynamics in Crystals

III-H-1 Femtosecond Pump-Probe Study of Coherent Soft Phonon in Ferroelectric Materilas

LU, Rong[1]; HASE, Muneaki[1]; KITAJIMA, Masahiro[2]; NAKASHIMA, Shinichi[3]; SUGAI, Shunji[4]
([1]NIMS; [2]NIMS, Univ. Tsukuba and IMS; [3]AIST; [4]Nagoya Univ.)

Structural phase transitions in solids have been investigated with X-ray- and neutron-scatterings, and especially through the "*soft mode*" dynamics using Raman scattering spectroscopy. However, such the soft mode is usually located at extremely low frequency or shifts to "zero" frequency when the lattice temperature approaches to the critical temperature T_c, which makes frequency-domain spectroscopic study difficult. For this point of view the time-domain spectroscopy method has advantage to study such low frequency phonon modes. The time-domain study provides also possibility of observing nonthermal phase transitions under high density photoexcitation above mJ/cm^2 pump fluences, which is inaccessible by frequency-domain techniques. Motivated by the observation of the ultrafast dynamics of structural phase transition in ferroelectric materials under the high-density photoexcitation, in this work, we have investigated the coherent soft mode in $Pb_{1-x}Ge_xTe$ (x = 0.07) using a pump-probe technique with amplified femtosecond laser pulses. As the pump fluence increases, the frequency of the coherent A_1 phonon becomes soften and at higher fluence it reaches saturation due to the screening effect in the electron-phonon interaction, while the large damping rate dose not show similar saturation due to the dominant anharmonic phonon-phonon coupling. The linear increase of the amplitude of the coherent phonon is ascribed to the linear increase of photo-excited carrier density under the DECP mechanism. The saturation behavior of the frequency of the soft mode implies that it will be difficult to realize the laser induced structural phase transition using single pump in $Pb_{1-x}Ge_xTe$, and multiple-pump excitation will provide a possibility for the future studies.

Reference

1) R. Lu, M. Hase, M. Kitajima, S. Nakashima and S. Sugai, *J. Lumin.* **378**, 119–120 (2006).

III-H-2 Temperature Dependence of Coherent A_{1g} and E_g Phonons of Bismuth

ISHIOKA, Kunie[1]; KITAJIMA, Masahiro[2]; MISOCHKO, O. V.[3]
([1]NIMS and Univ. Tsukuba; [2]NIMS, Univ. Tsukuba and IMS; [3]Russ. Acad. Sci.)

Bismuth has been a model material to study femtosecond dynamics of coherent lattice oscillations. The generation mechanism was considered to be displacive for the totally symmetric A_{1g} mode, which was the only coherent mode observed in the conventional (isotropic) detection. The absence of the other Raman active mode, E_g, has not been fully explained, but was phenomenologically attributed to the exclusive coupling of the hot electrons at $k < 0$ and high symmetry phonons. In the present study, we demonstrate that both A_{1g} and E_g modes are coherently excited at comparable amplitudes at low temperature, and thus proved that the coherent phonons are generated basically *via* Raman process. We found a puzzling $\pi/2$ difference in the initial phases of the two coherent oscillations, which suggests that the initial phase is not a clear-cut indication for the generation mechanism of the coherent phonons in absorbing media.

Reference

1) K. Ishioka, M. Kitajima and O. V. Misochko, *J. Appl. Phys.* **100**, 093501 (6 pages) (2006).

III-I In-Situ Observation of Surface Reactions by Variable Temperature Scanning Tunneling Microscopy

Chemical reactions at a well-defined single crystal surface has been intensively investigated as a prototype for heterogeneous catalytic reaction, electrochemical reaction and corrosion. The surface chemical reactions are heterogeneous in nature reflecting the structural and electronic imperfections relevant to steps, vacancies and impurities. In addition, the surface reactions are significantly influenced by the presence of reactants and products which often form ordered arrays. Therefore, in order to get better understanding of the surface reactions, it is vital to unravel the nature of these local properties which are closely linked to catalytic activity. The advent of scanning tunneling microscopy (STM) has enabled us to tackle the challenge with the ability to image the surface reactions in both real-time and real-space with atomic resolution. We investigate the reactivity of novel one-dimensional (1D) –Ag–O–Ag–O– compounds formed upon the dissociative adsorption of oxygen molecule on Ag(110) using variable temperature STM (VT-STM). The 1D compounds are arranged periodically to form (n×1) (n = 2–7) reconstructed structures. In addition, the 1D compounds show structural fluctuation in low O coverage regime reflecting the low dimensionality. These characteristics make them promising as a model system to explore physical and chemical properties of nano-structured materials.

III-I-1 Spontaneous Formation of Stripe Phase under the Dynamic Equilibrium between Adsorption and Desorption of H_2O on O-Covered Ag(110) Surfaces

TAKAGI, Noriaki[1]; NAKAGOE, Osamu[2]; WATANABE, Kazuya; MATSUMOTO, Yoshiyasu
([1]IMS and Univ. Tokyo; [2]Hokkaido Univ.)

The surface structure variation under the equilibrium condition achieved by the adsorption-desorption of H_2O ($H_2O + O_{(ad)} \leftrightarrow 2OH_{(ad)}$) on the Ag(110)(2×1)-O surface at room temperature was investigated using VT-STM. We found that the (2×1)-O and OH phase alternatively arrange to form periodic stripes. The STM observations were made by initially preparing the (2×1)-O surface and then exposing the surface to H_2O of $P_{H2O} = 1 \times 10^{-8}$ mbar. The initial surface is the (2×1)-O structure with small bare patches that are not covered with the AgO chains. These patches are randomly distributed and appear as darker lines. When the surface was exposed to H_2O, the darker lines wander and become frizzy because the deconstruction of AgO chains upon the reaction occurs at the boundary. In addition, the lines coalesce to extend from step to step, become bright and finally arrange periodically to form a stripe pattern. The average interval between the stripes was estimated to be 6–7 nm. When H_2O was fully evacuated, the stripe pattern became disordered and finally the structure similar to the initial structure was restored. This indicates that the spontaneous formation of the stripe pattern occurs only under the equilibrium.

The formation of phase boundary is generally unfavorable because energy cost related to the phase boundary increases the surface energy. Thus, the formation of the stripe pattern needs the energy gain which overcomes the energy cost accompanied by the interface formation. According to Vanderbildt,[1)] the interactions characterized by $1/r^3$ scaling are responsible for the stabilizing the stripe pattern formation. The elastic and electrostatic interactions bewteen the (2×1)-O and the OH phases are dominant candidates. Simple estimation based on the theory suggests that the energy gain originating from the electrostatic interaction is not sufficient and thus the elastic relaxation is responsible for the formation of the stripe pattern.

Reference

1) D. Vanderbilt, *Surf. Sci.* **268**, L300 (1992).

III-I-2 Direct Observation of a Propagating Chemical Wave in Disproportionation Reactions of Water on Oxidized Ag(110) Surface by Scanning Tunneling Microscopy

TAKAGI, Noriaki[1]; NAKAGOE, Osamu[2]; WATANABE, Kazuya; MATSUMOTO, Yoshiyasu
([1]IMS and Univ. Tokyo; [2]Hokkaido Univ.)

Scanning tunneling microscopy was used for studying spatiotemporal evolution of the disproportionation reaction of H_2O with O adatoms on oxidized Ag(110) surfaces where quasi-one dimensional AgO chains form ordered structures. Initially the reaction takes place slowly on Ag(110)-(5×1)O at the end of AgO chain, whereas the reaction accelerates explosively upon the appearance of a chemical wave that propagates along the direction perpendicular to the chain. The surface morphology of the region swept over by the chemical wave completely changes from (5×1)-O to that with many rectangular islands, indicating the formation of $H_2O(OH)_2$. The induction time and explosive acceleration with the propagating chemical wave imply that the reaction is autocatalytic. Water clusters hydrating OH produced likely play a central role in serving as a reservoir of H_2O to feed to the reaction and enhancing the reactivity of H_2O with O adatoms in AgO chains.

III-J High-Resolution Spectroscopy and Excited-State Dynamics of Jet-Cooled Molecules

The energy structures in the electronic excited states of isolated molecules are of great importance. The excited-state dynamics such as internal conversion to the ground state (IC), intersystem crossing to the triplet state (ISC), intramolecular vibrational redistribution (IVR), vibronic interaction, and predissociation are closely related with the irregular changes of the energy levels, *i.e.*, perturbations. High-resolution laser spectroscopy is one of the powerful methods to investigate the perturbation between the electronic states. The aims of this project are to accurately observe the fluorescence and phosphorescence excitation spectra in a supersonic jet and rotationally resolved spectra of isolated molecules using a new system of coherent narrowband pulse laser light.

In aromatic hydrocarbons such as benzene, naphthalene, and anthracene, the ISC is not expected to be a major process. In contrast with this, the triplet state plays an important role in molecules with the nπ* lowest state such as aldehydes and ketones. The dynamical processes can be understood by analyzing rovibronic structure in the high-resolution spectrum.

III-J-1 Vibronic Structure in the S_1–S_0 Transition of Jet-Cooled Dibenzofuran

BABA, Masaaki[1]; MORI, Koichi[2]; YAMAWAKI, Michiru[3]; KASAHARA, Shunji[3]; YAMANAKA, Takaya
([1]IMS and Kyoto Univ.; [2]Kyoto Univ.; [3]Kobe Univ.)

[*J. Phys. Chem. A* **110**, 10000–10005 (2006)]

Dibenzofuran is one of the prototypical molecules of toxic dioxins.[1)] We have observed the fluorescence excitation spectrum and dispersed fluorescence spectrum of the S_1–S_0 transition of jet-cooled dibenzofuran. We observed strong vibronic bands whose intensities are larger than the 0–0 band. The observed vibronic bands were assigned referring to *ab initio* calculations of the normal vibrations. The molecule is essentially planar and the structure is not much changed by the electronic excitation. It is concluded that intensities of the observed strong vibronic bands arise from vibronic interaction between the S_1 $^1A_1$ and S_2 $^1B_2$ ππ* states. The energies of b_2 vibrational bands are decreased by the vibronic interaction. Broad component was observed in the dispersed fluorescence spectrum. It indicates that IVR occurs in the lower energy vibronic levels of the S_1 state.

Reference

1) M. Baba *et al., J. Phys. Chem. A* **108**, 1388–1392 (2004).

III-J-2 Energy Levels of CH_3 Rotation in the S_1 and S_0 States of 9-Methylanthracene

BABA, Masaaki[1]; MORI, Koichi[2]; YAMANAKA, Takaya
([1]IMS and Kyoto Univ.; [2]Kyoto Univ.)

CH_3 internal rotation induces radiationless transitions of aromatic molecules. In order to understand the mechanism of excited-state dynamics of methyl containing molecules we have observed high-resolution spectra of jet-cooled 9-methylanthracene (9MA). We found several low energy bands, which are assigned to transitions between the vibrational levels of CH_3 internal rotation. The barrier height to CH_3 rotation was estimated to be about 100 and 50 cm^{-1} in the S_0 and S_1 states, respectively. The barrier height is attributed to steric repulsion and interaction with the π orbitals. The barrier height is very small in toluene and that in 9MA is relatively larger. This increase is considered to be due to larger anisotropy of the π orbitals in 9MA.

The dispersed fluorescence spectra indicate that IVR occurs in the lower energy vibrational levels of the S_1 state. The threshold is much smaller than that of anthracene. The IVR is considered to be enhanced by CH_3 substitution. It is the effect of increase of the level density, lowering of the symmetry, and coupling of the out-of-plane vibrations.

III-J-3 High-Resolution Spectroscopy of the T_1 $^3A_u(n\pi^*)$ State of Oxalyl Chloride

BABA, Masaaki[1]; HASEGAWA, Hirokazu; OHSHIMA, Yasuhiro
([1]IMS and Kyoto Univ.)

Oxalyl Chloride is a Cl derivative of glyoxal which is a prototypical diketones. Generally energy difference between the nπ* and ππ* states are very small in diketones and ISC occurs efficiently in the S_1 state. The energy structure of the triplet state is an important factor to quantitatively understand the mechanism. In order to observe high-resolution spectrum, strong pulse laser light is necessary because the S–T transition is very weak. In particular Cl atoms enhance radiationless transitions which are called as heavy atom effect. Furthermore, there are two mass isotopes of the Cl atom and the spectrum becomes congested.

Phosphorescence of jet-cooled oxalyl chloride was observed and an S–T phosphorescence excitation spectrum has been reported using a pulse laser with the resolution of 0.2 cm^{-1}.[1)] Pulse amplifing of CW single-mode laser makes it possible to observe rotationally resolved spectrum. The three spin sublevels in the triplet state and the coupling with the rotation angular momentum are important to understand the mechanism of ISC.

Reference

1) T. Yoshii *et al., J. Phys. Chem.* **100**, 3354–3358 (1996).